DOI: 10.1002/cplu.201200281

Synthesis of Anatase Se/Te-TiO_2 Nanorods with Dominant {100} Facets: Photocatalytic and Antibacterial Activity Induced by Visible Light

Zong-Hong Lin, Prathik Roy, Zih-Yu Shih, Chung-Mao Ou, and Huan-Tsung Chang*[a]

A facile method for the preparation of Te- and Se/Te-doped anatase TiO_2 nanorods (NRs) with exposed {100} facets, which provides high photocatalytic and antibacterial activity under irradiation with visible light, is developed. Sodium titanate nanotubes are formed from commercial TiO_2 nanoparticles (P25) in NaOH through a hydrothermal reaction. The as-prepared Na-titanate nanotubes are then used to form Te-TiO_2 nanotubes in the presence of tellurite (TeO_3^{2-}) ions and $NaBH_4$. Upon further hydrothermal reaction, the Te-TiO_2 nanotubes are transformed to form Te-TiO_2 NRs that further form Se_n/Te-TiO_2 NRs through a reduction of selenite (SeO_3^{2-}) ions with $NaBH_4$. The Te-TiO_2 NRs and Se_n/Te-TiO_2 NRs have highly active {100} facets and thus provide the photocatalytic activities for the generation of ·OH at 2.5 and 4.5 times higher than that of commercial P25, respectively. The Te-TiO_2 and Se_n/Te-TiO_2 NRs exhibit higher antibacterial activities against *E. coli* and *S. aureus* than P25 when activated by visible light. These stable and biocompatible Te-TiO_2 and Se_n/Te-TiO_2 NRs hold great potential as potent antibacterial agents.

Introduction

Titanium dioxide has great potential application in a wide range of fields such as photocatalysis, solar energy, and gas sensing, originating from its unique physical and chemical properties.[1–3] Inexpensive TiO_2 is stable with respect to photocorrosion and chemical corrosion over prolonged periods of time. In addition, TiO_2 is a good semiconductor photocatalyst for the degradation of organic compounds, mainly because the redox potential of the H_2O/·OH couple ($OH^- = OH + e^-$; $E^o = -2.8$ V) lies within its band gap.[4] These properties depend on their size, shape, and crystal phase.[5–7] Among all TiO_2 crystal phases, anatase TiO_2 provides excellent applications.[8] Theoretical calculations have indicated that the {001} and {100} facets of anatase TiO_2 are active facets with high surface energies, whereas the thermodynamically most stable surface facets are {101}.[9] According to the Wulff construction, the equilibrium shape of an anatase crystal is enclosed by the most stable {101} facets that account for 94% of the total surface, leading to limited activity for anatase crystals.[10] To enhance the activity of TiO_2, strategies for the synthesis of well-defined anatase crystals with a large percentage of exposed high-energy {001} or {100} facets have been proposed.[11] For example, TiO_2 nanocuboids[12] and nanorods[13] with large percentages of {100} facets exhibited higher photocatalytic activity (three times) than the commercial P25 for the reaction with hydroxyl radicals (·OH).[14] Dye-sensitized solar cells featuring TiO_2 photoanodes with about 10%, 38%, and 80% exposed {001} facets provided overall conversion efficiencies of 7.47%, 8.14%, and 8.49%, respectively.[15]

Alternatively, the photocatalytic activity of TiO_2 can be enhanced by doping with transition metals such as silver, gold, and platinum.[16] Traditional TiO_2 (band gap 3.0 eV for rutile and 3.2 eV for anatase) photocatalysts is effective only upon irradiation of UV light, with potential damage to human cells.[17] To provide photocatalytic activity induced by visible light, TiO_2 nanoparticles (NPs) doped with metallic species and nonmetallic species such as carbon, nitrogen, sulfur, and silver have also been prepared.[18–21] Among them, silver-doped TiO_2 NPs are the most attractive for the antibacterial application.[20,21] However, concern about their toxicity to animals and cells has been raised.[22] Thus, preparation of biologically friendly and cost-effective antibacterial agents is essential.

Herein, we prepared anatase TiO_2 nanorods (NRs) having large active {100} facets that were further doped with tellurium and selenium through hydrothermal reactions. Selenium NPs[23] possessed strong ability to inhibit the growth of *Escherichia coli* (*E. coli*) and *Staphylococcus aureus* (*S. aureus*), whereas tellurite (TeO_3^{2-}) ions and Te nanomaterials (NMs) effectively inhibited the growth of penicillin-insensitive bacteria.[24] The capability of generation of hydroxyl radicals (·OH) of the as-prepared Se_n/Te-TiO_2 NRs in aqueous solution and their antibacterial activity against *E. coli* and *S. aureus* under irradiation with visible light were evaluated.

[a] *Dr. Z.-H. Lin, P. Roy, Z.-Y. Shih, Dr. C.-M. Ou, Prof. H.-T. Chang*
Department of Chemistry
National Taiwan University
1, Section 4, Roosevelt Road, Taipei 106 (Taiwan)
Fax: (00886) 011-886-2-33661171
E-mail: changht@ntu.edu.tw

Supporting information for this article is available on the WWW under http://dx.doi.org/10.1002/cplu.201200281.

Results and Discussion

Synthesis of Se_n/Te-TiO_2 NRs

Sodium titanate nanotubes were prepared from TiO_2 NPs (P25) on a large scale through a hydrothermal route to give nanoparticles of uniform morphology.[25] Two main mechanisms that have been suggested for the formation of Na-titanate nanotubes are: 1) rolling of Na-titanate nanosheets (100) along the [010] direction,[26] and 2) bending and folding of Na-titanate multisheets.[27] The TEM image depicted in Figure 1A reveals the formation of Na-titanate nanotubes, with (13.8 ± 4.3) nm in diameter and (6.1 ± 1.9) μm in length. The reduction of the adsorbed TeO_3^{2-} ions on the Na-titanate nanotubes with $NaBH_4$ at 25 °C resulted in the formation of Te-TiO_2 nanotubes, which were further transformed into Te-TiO_2 NRs (Figure 1B) at 200 °C. Transformation of Na-Titanate nanotubes into anatase TiO_2 NRs in a basic medium by using a hydrothermal method has been reported.[13] Through acid or centrifugation treatment, most of the adsorbed sodium ions on titanate nanotubes were removed. In this study, the adsorbed sodium ions were replaced by Te^{4+} ions, leading to decreases in the solution pH value from 13.0 to 9.5. The Te^{4+} ions were further reduced by $NaBH_4$ to form a part of the crystal lattices during the transformation of Te-titanate nanotubes to Te-TiO_2 NRs. The SEM image depicted in the inset to Figure 1B displays that the NRs had well-defined lateral facets with sharp edges and adjacent perpendicular facets, with width (106 ± 13) nm and length (824 ± 115) nm. Elemental mapping images of Ti, O, and Te on a single Te-TiO_2 NR (Figure 1C) obtained by applying a high-angle annular dark-field scanning TEM energy-dispersive X-ray spectroscopy (HAADF-STEM-EDX) reveal that Ti, O, and Te signals are well distributed throughout the NRs. The high-resolution (HR) TEM image (Figure 1D) recorded along the [001] direction of the Te-TiO_2 NRs shows three sets of lattice fringes with spacings of 4.8, 3.5, and 3.5 Å, which are assigned to {002}, {101}, and {10$\bar{1}$} facets, respectively. Along with the SEM and TEM images, and the crystallographic symmetries of TiO_2 anatase, the surfaces of these well faceted Te-TiO_2 NRs are identified as lateral {100}, {101}, and top {001} (inset in Figure 1B). We point out that the {100} facets of the as-prepared Te-TiO_2 NRs are the main exposed lateral facets. To investigate the formation of Te-TiO_2 NRs from Te-TiO_2 nanotubes, we recorded time evolution SEM images (Figure S1 in the Supporting Information) over the course of the reaction (0–12 h). Some NPs became apparent at the reaction time of 4 hours, meanwhile the NPs gradually grew up and the length of nanotubes decreased over the reaction period of 4–8 hours. The formation of the Te-TiO_2 NRs was completed at the reaction time of 12 hours. The transformation process proceeded through dissolution and nucleation. At the beginning, the surfaces of Te-TiO_2 nanotubes gradually decomposed to produce $Ti(OH)_4$ fragments and hydroxy ions.[9] Then, the $Ti(OH)_4$ fragments rearranged to share edges through a dehydration reaction, resulting in the formation of anatase seeds. Subsequently, $Ti(OH)_4$ fragments diffused to the surface of the TiO_2 seeds to form larger TiO_2 NPs. Because the hydroxy ions gradually released from nanotubes and preferentially adsorbed onto anatase (100) facets, lowering the surface energy of (100) facets, and directing the crystal growth along the a- and b-axis.[23]

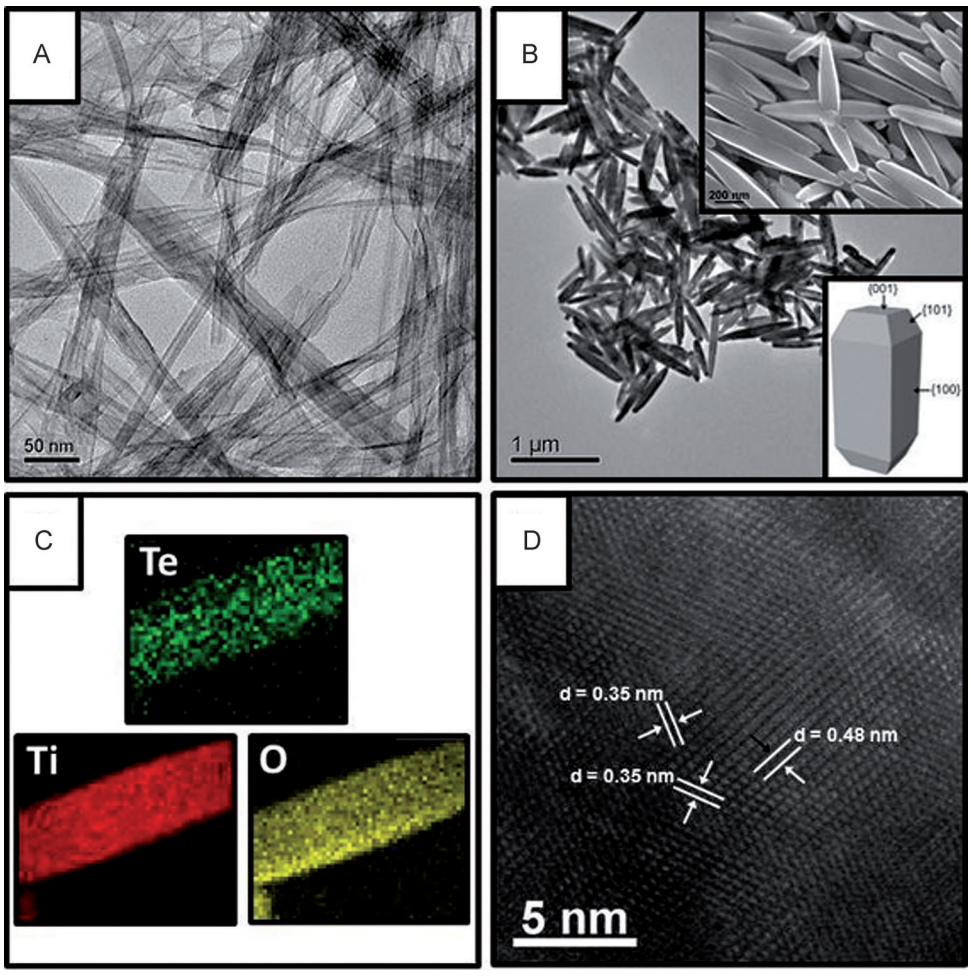

Figure 1. TEM images of the (A) Na-titanate nanotubes and (B) Te-TiO_2 NRs. Inset to (B): SEM image of Te-TiO_2 NRs. (C) HAADF-STEM-EDX mapping of one representative Te-TiO_2 NR for Ti, O, and Te elements, separately. (D) HRTEM image of Te-TiO_2 NRs.

To increase the photocatalytic activity of the as-prepared Te-TiO_2 NRs in the visible region, we used selenium as a second

doping element based on that fact that it can shift the absorption to the visible as a result of its small band gap (2.0 eV).[28] In addition, selenium itself can also generate the electron-hole pairs and thus Se NPs have been used for degradation of organic dyes under illumination.[29] Furthermore, TiO_2 and selenium can form an n-TiO_2/p-Se diode in which the photocurrent is produced by transferring electron from TiO_2 to selenium when exposed to visible light (Figure S2).[30] We carried out a controlled experiment using SeO_3^{2-} ions instead of TeO_3^{2-} ions for the synthesis of Se-TiO_2 NRs. However, only spherical Se NPs and TiO_2 NPs were obtained, mainly because the melting point of Se is low (217 °C). In other words, some of Se atoms might be melted from the surfaces of TiO_2 nanotubes during the hydrothermal reaction (200 °C). By controlling the concentration of selenite (SeO_3^{2-}) ions, we prepared Se_n/Te-TiO_2 NRs containing different amounts of Se atoms through a reduction mediated by $NaBH_4$. The ICP-MS measurements revealed that the weight percentages of Se in the three samples of Se_n/Te-TiO_2 NRs are 1.8, 5.2, and 6.5% when using SeO_3^{2-} ions of 2, 5, and 10 mM as the precursors, respectively. The percentages of Te in the Te-TiO_2 NRs and three Se_n/Te-TiO_2 NRs were all around 5.7%. For simplicity, the three as-prepared Se_n/Te-TiO_2 NRs are represented as $Se_{0.02}$/Te-TiO_2, $Se_{0.05}$/Te-TiO_2, and $Se_{0.07}$/Te-TiO_2 NRs, respectively. The SEM image, EDX spectrum, TEM image, and HAADF-STEM-EDX of $Se_{0.07}$/Te-TiO_2 NRs as shown in Figure S3, reveal that the morphology of $Se_{0.07}$/Te-TiO_2 NRs did not change during the process of Se reduction, and Te and Se were both present in $Se_{0.07}$/Te-TiO_2 NRs.

Figure 2A shows the XRD patterns of commercial TiO_2 NPs (P25), Na-titanate nanotubes, Te-TiO_2 NRs, and the as-prepared Se_n/Te-TiO_2 NRs. The characteristic facets of {101}, {103}, {004}, {112}, {200}, {105}, and {211} are assigned for the anatase crystal phase, and facets {110} and {101} corresponds to the rutile crystal phase, revealing the presence of anatase and rutile TiO_2 crystal phases in the P25 sample (curve a). On the other hand, no anatase or rutile peaks are assigned in the Na-TiO_2 nanotubes (curve b). In contrast, the diffraction peaks of Te-TiO_2 and $Se_{0.07}$/Te-TiO_2 NRs reveal that their structures are mainly anatase phases (curves c and d). The Raman spectra shown in Figure 2B further confirm the XRD results. The strong peaks at 139, 192, 392, 511, and 635 cm^{-1} correspond to the anatase phase and the weak shoulder at 441 cm^{-1} is a characteristic peak of the rutile phase, thereby supporting the observation that P25 has both phases. The Na-TiO_2 nanotubes did not show these characteristic Raman peaks. The five Raman modes with strong intensities at 140, 196, 390, 514, and 632 cm^{-1} for the Te-TiO_2 and $Se_{0.07}$/Te-TiO_2 NRs further confirmed that their structures are mainly anatase phases. The peaks at 122 and 266 cm^{-1} are assigned to the Te lattice vibration and Te-O vibration of the oxide layer,[31] while the peak at 256 cm^{-1} corresponds to amorphous Se vibration.[32] The chemical compositions of the as-prepared $Se_{0.07}$/Te-TiO_2 NRs were further confirmed by conducting XPS measurements. Figure 3 reveals the existence of Se, Te, and Ti in the $Se_{0.07}$/Te-TiO_2 NRs. The binding energies of Ti $2p_{3/2}$ and Ti $2p_{1/2}$ are at 458.4 and 464.1 eV, respectively (Figure 3A), indicating a similar oxidation state of the Ti element to that of bulk TiO_2.[33] The peaks at 572.5 and 582.4 eV correspond to Te $3d_{5/2}$ and Te $3d_{3/2}$ (Figure 3B), respectively. Meanwhile the two peaks at 575.6 and 586.0 eV are attributed to tellurium(IV) oxide.[34] The TeO_2/Te ratio is 0.67, revealing the formation of tellurium oxide on the surfaces of the Te-TiO_2 NRs as a result of their highly reactive and easily oxidizable properties.[35] The peaks at 54.9 eV and 61.7 eV are assigned for Se 3d (atom) and Ti 3s, respectively.

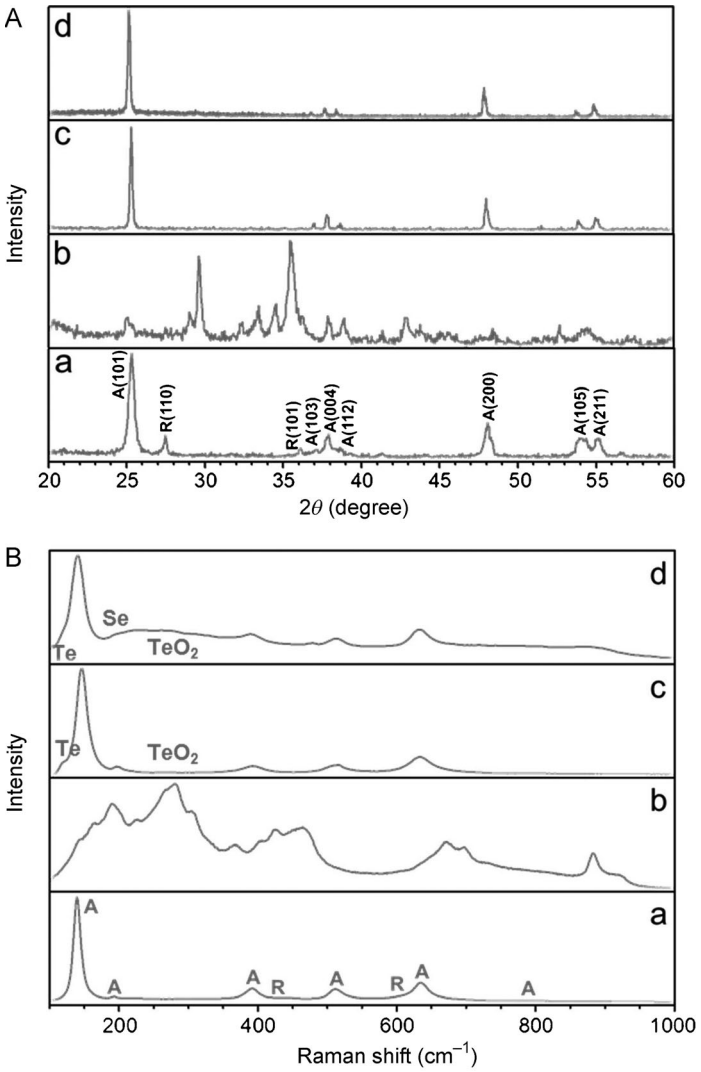

Figure 2. (A) XRD and (B) Raman spectra of the (a) TiO_2 NPs, (b) Na-titanate nanotubes, (c) Te-TiO_2 NRs, and (d) $Se_{0.07}$/Te-TiO_2 NRs.

Photocatalytic activities of the as-prepared nanomaterials

Figure 4A displays the UV/Vis absorption spectra of the TiO_2 NPs, Te-TiO_2 NRs, and Se_n/Te-TiO_2 NRs. The doping of elementary Te into the TiO_2 lattice induced a shift of the maxi-

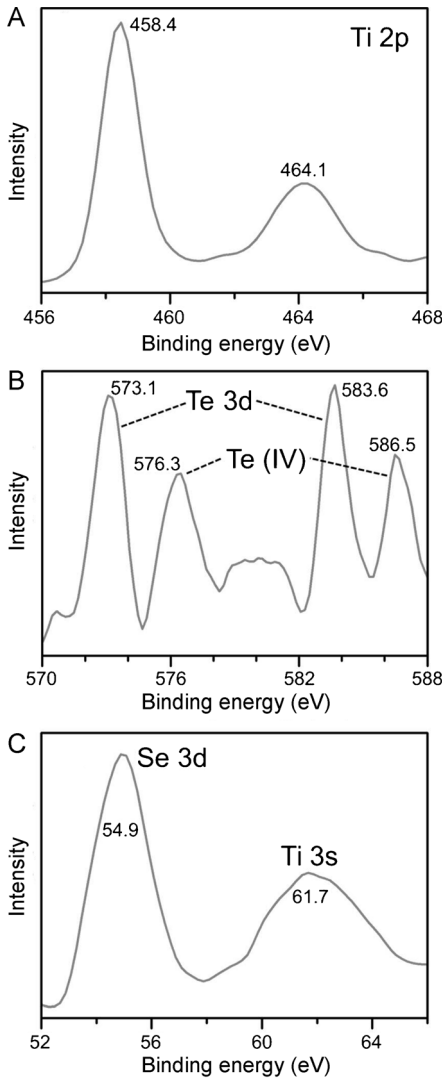

Figure 3. XPS spectra of $Se_{0.07}$/Te-TiO_2 NRs. (A) Ti, (B) Te, and (C) Se and Ti.

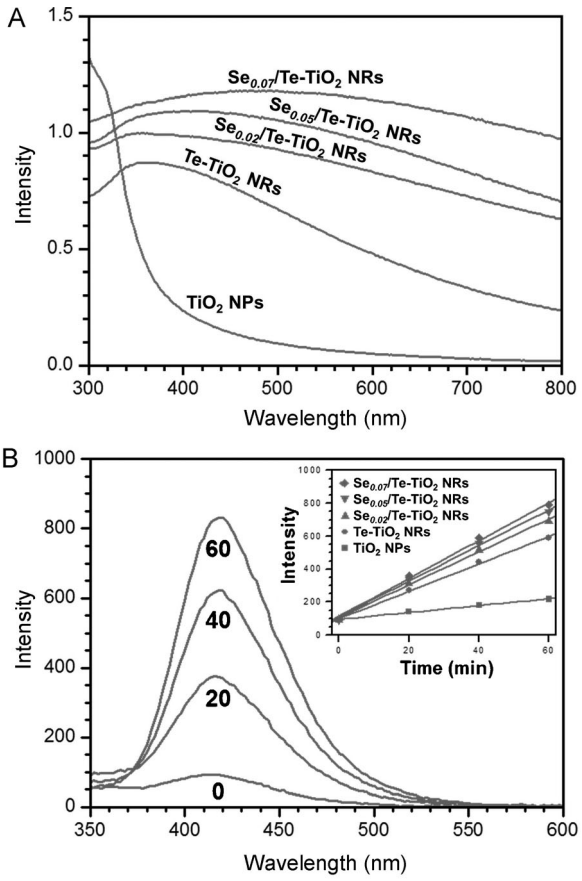

Figure 4. (A) Absorption spectra of TiO_2 NPs, Te-TiO_2 NRs, and three Se_n/Te-TiO_2 NRs. (B) Changes in the fluorescence of TA solution under light irradiation in the presence of the $Se_{0.07}$/Te-TiO_2 NRs. Inset to (B): comparison of photocatalytic activity of the four as-prepared NMs and TiO_2 NPs.

mum absorption wavelength from 300 to 350 nm; this shift occurs because Te has a smaller band gap than that of TiO_2 (0.3 vs. 3.2 eV).[36] The growth of Se to Te-TiO_2 NRs further enhanced the absorbance in the visible-light region (nominal wavelength at 500 nm). Upon increasing the content of Se in the Se_n/Te-TiO_2 NRs, the absorbance increased. The long-tail absorption in the visible region (500–800 nm) was attributed to the absorption of the selenium thin layer or NPs.[29] The photocatalytic activities of TiO_2 NPs, Te-TiO_2 NRs, and Se_n/Te-TiO_2 NRs were evaluated by measuring the formation of active ·OH upon irradiation.[37] Figure 4B displays the fluorescence spectra of the mixtures of terephthalic acid (TA; 3 mM), NaOH (10 mM), and $Se_{0.07}$/Te-TiO_2 NRs that had been irradiated under visible light for various periods of time. To start, TA is nonfluorescent whereas upon reaction with ·OH its product (2-hydroxyterephthalic acid; TAOH) has strong fluorescence at 420 nm. Upon increasing irradiation time, the fluorescence intensity of the solution at 420 nm increased gradually. The $Se_{0.07}$/Te-TiO_2 NRs provided about 4.5 and 1.8 times higher photoactivity than that of the TiO_2 NPs and Te-TiO_2 NRs, respectively. To provide further evidence of the formation of its product TAOH during the photocatalytic process, we conducted electrospray ionization mass spectrometry (ESI-MS) as shown in Figure S4. The product TAOH was detected after 60 minutes of reaction time. We also compared the photocatalytic activity of the as-prepared Te-TiO_2 and Se_n/Te-TiO_2 NRs by using the same concentration of NRs (Figure S5). All these results indicate that the Se contributes to the enhanced photocatalytic activity. The anatase TiO_2 NRs with exposed {100} facets[13] relative to TiO_2 NPs provided greater photocatalytic activity (Figure S6). The enhanced photocatalytic activity of Te-TiO_2 NRs compared to TiO_2 NPs is a result of the structure effect (dominant {100} facets) and changes in the electronic state.[38–41]

As a control, solutions containing TA (3 mM) and NaOH (10 mM) in the presence of TeO_3^{2-} ions, SeO_3^{2-} ions, Te nanowires (NWs), or Se NPs were subjected to irradiation under the same conditions (Figure S7). In the absence of the ions and NMs, the fluorescence intensity was nearly constant over the irradiation period. These results reveal that the formation of TAOH was due to the reaction of TA and ·OH generated from the NMs during the photocatalytic process.[42] Among the ions used and NMs, Se NPs provided the most strong photocatalytic activity; however, the activity is less than 10% of the $Se_{0.07}$/Te-

TiO_2 NRs. The Te NWs and TeO_3^{2-} ions showed less than 10% of the photocatalytic activity of that of Te-TiO_2 NRs (Figure S7). Upon increasing the concentration of the as-prepared NMs from 100 μg to 10 mg, their photocatalytic activity (TAOH formation) increased as shown in Figure S8.

Antibacterial properties of the as-prepared NMs

Antibacterial properties of the five NMs against *E. coli* and *S. aureus* were investigated. Representative microscopic images of *E. coli* in lysogeny broth (LB) media that had been incubated in the presence and absence of $Se_{0.07}$/Te-TiO_2 NRs under visible-light irradiation for 60 minutes are depicted in Figure 5 A,B. The green and red images correspond to live and dead *E. coli*, respectively. The percent viability values of the *E. coli* cells in the media in the absence of any NMs, and in the presence of one of the five NMs with/without being subjected to irradiation for 60 minutes are plotted in Figure 5 C,D. Live/dead ratios of bacteria were used to represent the antibacterial activity. The fluorescence approach allowed counting all bacteria at the same time, thus providing more reliable data than those determined by counting the bacteria under a microscope.

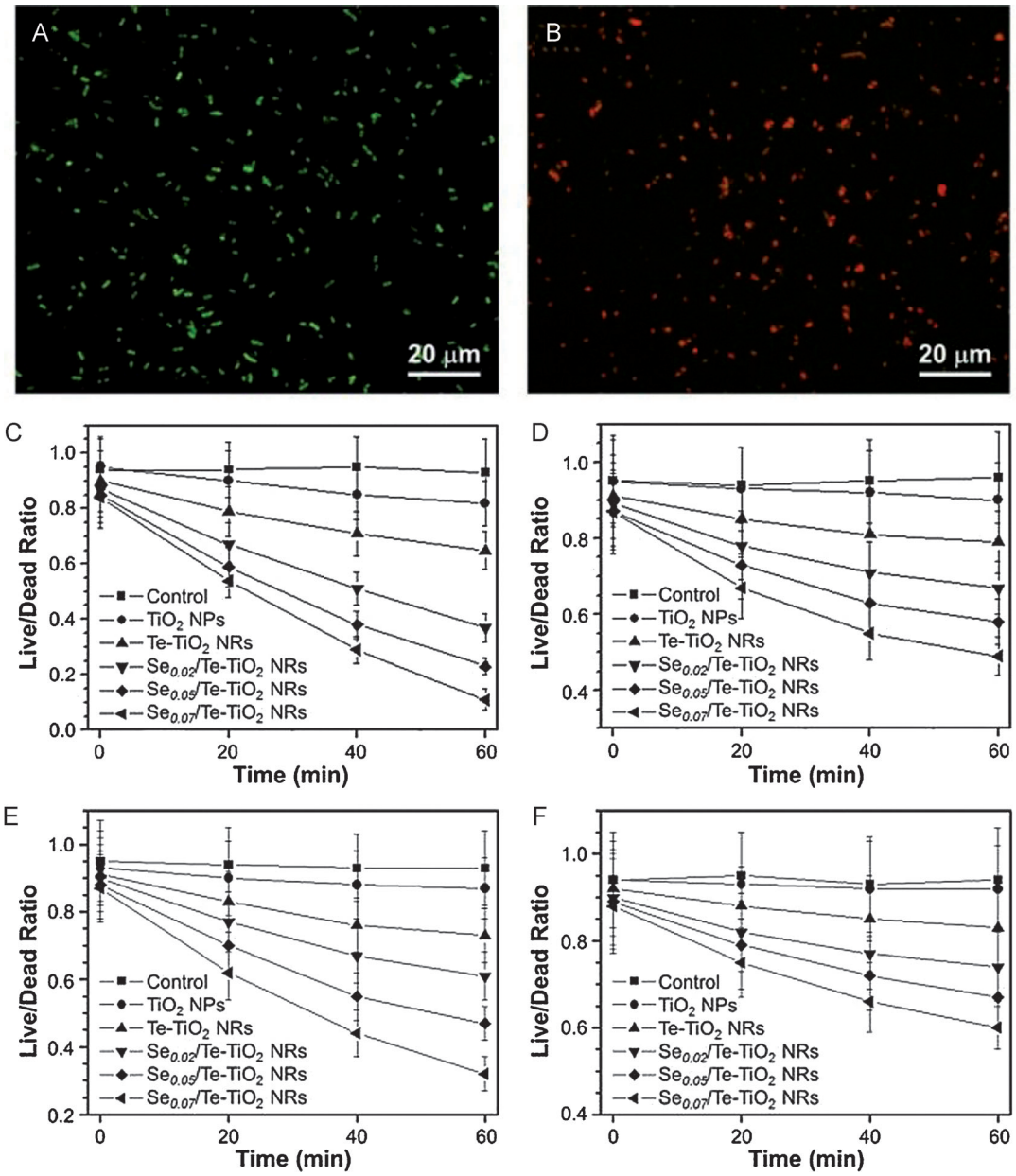

Figure 5. Fluorescence images of *E. Coli* in LB media irradiated under visible light without (A) and with (B) $Se_{0.07}$/Te-TiO_2 NRs for 1 h. *E. Coli* cells were stained with SYTO 9/PI. Green fluorescent stains are representative of live cells while red fluorescent stains are representative of dead or compromised cells. (C) and (D): live/dead cell ratios of *E. Coli* in LB media incubated with as-prepared NMs and TiO_2 NPs under (C) irradiation with visible light or (D) in the dark. Live/dead cell ratios of *S. aureus* in LB media incubated with the as-prepared NMs and TiO_2 NPs under (E) light irradiation or (F) in the dark. The live/dead ratios were calculated from the fluorescence measurement according to the manufacturer's guide of the BacLight Bacterial Viability and Counting Kit from Invitrogen. The control experiments are the cells under irradiation with visible light or in the dark in the absence of any of the NMs.

Under visible-light irradiation (Figure 5C), the decreasing order of the viability of *E. coli* was $TiO_2 > Te\text{-}TiO_2 > Se_{0.02}/Te\text{-}TiO_2 > Se_{0.05}/Te\text{-}TiO_2 > Se_{0.07}/Te\text{-}TiO_2$. After 60 minutes, the viability values were 83, 65, 37, 23, and 11% in the presence of TiO_2, $Te\text{-}TiO_2$, $Se_{0.02}/Te\text{-}TiO_2$, $Se_{0.05}/Te\text{-}TiO_2$, and $Se_{0.07}/Te\text{-}TiO_2$ NMs (all 100 μg mL^{-1}), respectively. All three $Se/Te\text{-}TiO_2$ NRs provided live/dead ratios of *E. coli* less than 0.4 within 1 hour after irradiation with visible light. Without light irradiation (Figure 5D), the decreasing order of the viability of *E. coli* in the presence of various NMs was $TiO_2 > Te\text{-}TiO_2 > Se_{0.02}/Te\text{-}TiO_2 > Se_{0.05}/Te\text{-}TiO_2 > Se_{0.07}/Te\text{-}TiO_2$. After 60 minutes, the viability values were 90, 79, 67, 58, and 49% in the presence of TiO_2, $Te\text{-}TiO_2$, $Se_{0.02}/Te\text{-}TiO_2$, $Se_{0.05}/Te\text{-}TiO_2$, and $Se_{0.07}/Te\text{-}TiO_2$ NMs (all 100 μg mL^{-1}), respectively. The antibacterial activity of these compounds in vitro is due to the strong oxidative nature of tellurium and/or selenium elements.[43] The antibacterial activities of the NMs against *S. aureus* are shown in Figure 5E,F with/without being subjected to irradiation with visible light. Under this irradiation (Figure 5E), the decreasing order of the viability of *S. aureus* was $TiO_2 > Te\text{-}TiO_2 > Se_{0.02}/Te\text{-}TiO_2 > Se_{0.05}/Te\text{-}TiO_2 > Se_{0.07}/Te\text{-}TiO_2$. After 60 minutes, the viability values were 87, 73, 61, 47, and 32% in the presence of TiO_2, $Te\text{-}TiO_2$, $Se_{0.02}/Te\text{-}TiO_2$, $Se_{0.05}/Te\text{-}TiO_2$, and $Se_{0.07}/Te\text{-}TiO_2$ NMs (all 100 μg mL^{-1}), respectively. The decreasing order of the viability of *S. aureus* in the presence of the NMs was $TiO_2 > Te\text{-}TiO_2 > Se_{0.02}/Te\text{-}TiO_2 > Se_{0.05}/Te\text{-}TiO_2 > Se_{0.07}/Te\text{-}TiO_2$ without visible-light irradiation (Figure 5F). After 60 minutes, the viability values were 92, 83, 74, 67, and 60% in the presence of TiO_2, $Te\text{-}TiO_2$, $Se_{0.02}/Te\text{-}TiO_2$, $Se_{0.05}/Te\text{-}TiO_2$, and $Se_{0.07}/Te\text{-}TiO_2$ NMs (all 100 μg mL^{-1}), respectively. The antibacterial activity of traditional TiO_2 NPs results from the formation of reactive oxygen species (ROS).[44] The ROS generation on or near the TiO_2 surface causes oxidative damage to cell membranes and inactivate microorganisms. Our results revealed that the as-prepared $Te\text{-}TiO_2$ and $Se_n/Te\text{-}TiO_2$ NRs generated greater amounts of ·OH and thus provided higher photocatalytic activity than the commercial TiO_2 NPs upon irradiation. In the dark, the TiO_2 NPs show nearly no activity, but the $Te\text{-}TiO_2$ and $Se_n/Te\text{-}TiO_2$ NRs both had strong activity.

To further understand the antibacterial properties of the as-prepared $Te\text{-}TiO_2$ and $Se_n/Te\text{-}TiO_2$ NRs against the bacteria, the ions released from the $Te\text{-}TiO_2$ and $Se_n/Te\text{-}TiO_2$ NRs in the presence of *E. Coli* in the LB media over different times as well as with or without with visible light were investigated (Figure 6). The ICP-MS data reveal that after irradiation for 60 minutes the concentrations of the released TeO_3^{2-} ions were nearly 45 ppb for $Te\text{-}TiO_2$ and three $Se_n/Te\text{-}TiO_2$ NRs, and the concentrations of the released SeO_3^{2-} ions from the $Se_{0.02}/Te\text{-}TiO_2$, $Se_{0.05}/Te\text{-}TiO_2$, and $Se_{0.07}/Te\text{-}TiO_2$ NRs were 17, 29, and 53 ppb, respectively. These results indicate that the $Se_n/Te\text{-}TiO_2$ NRs relative to $Te\text{-}TiO_2$ NRs provided greater antibacterial activity, mainly owing to the presence of selenium and the released SeO_3^{2-} ions. The concentrations of the released ions were almost the same

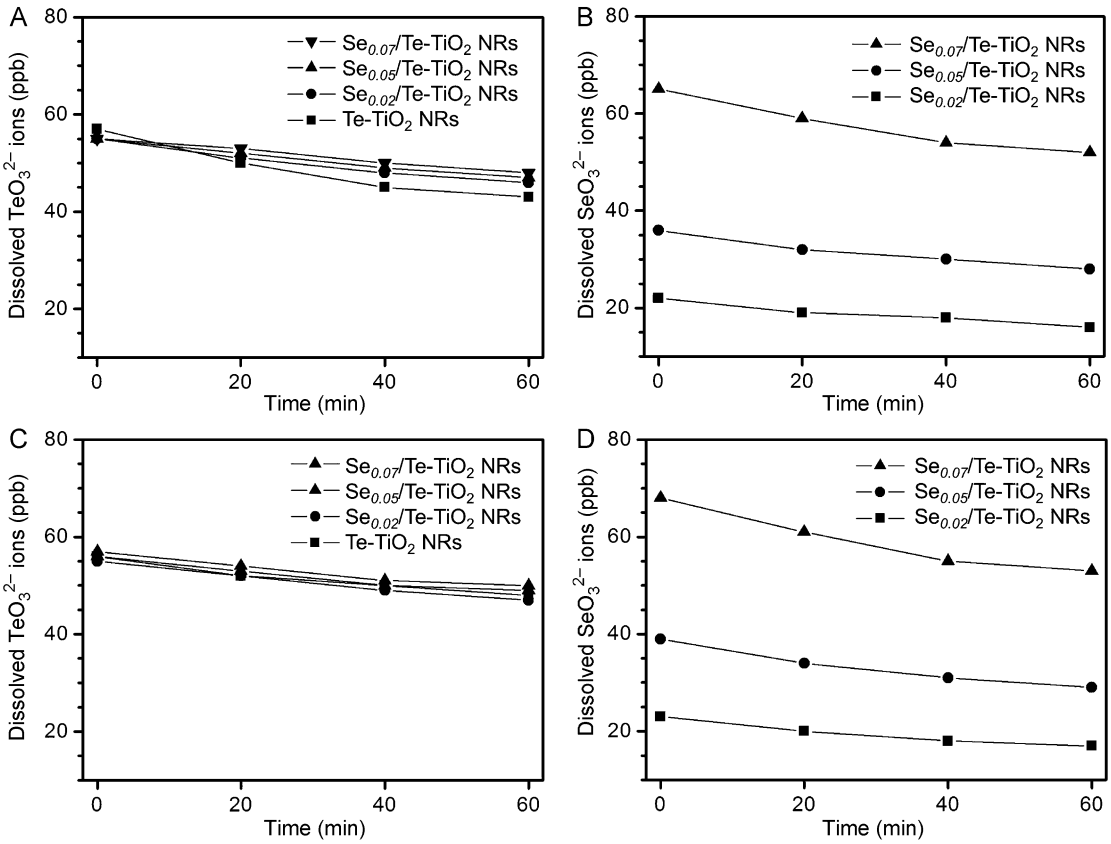

Figure 6. Dissolved TeO_3^{2-} and SeO_3^{2-} ions from $Te\text{-}TiO_2$ and $Se_n/Te\text{-}TiO_2$ NRs during the bactericidal processes in LB media for 1 h. (A) and (B): irradiated with visible light; (C) and (D): in the dark.

under irradiation with visible light or in the dark. The concentrations of TeO_3^{2-} and SeO_3^{2-} ions in the media decreased gradually over 0–60 minutes. The decreasing order of the released SeO_3^{2-} ions from the Se_n/Te-TiO_2 NRs was $Se_{0.07}$/Te-TiO_2 > $Se_{0.05}$/Te-TiO_2 > $Se_{0.02}$/Te-TiO_2. This order is consistent with the result of the antibacterial activity in the dark. Thus, the antibacterial activities of Se_n/Te-TiO_2 NRs were also analogous to the released TeO_3^{2-} and SeO_3^{2-} ions, which are toxic to most microorganisms mainly because of their strong oxidative nature.[45] The results reveal that the formation of TeO_3^{2-} and SeO_3^{2-} ions is mainly responsible for the antibacterial activity of the Se_n/Te-TiO_2 NRs in the dark. Because the concentrations of the released TeO_3^{2-} and SeO_3^{2-} ions were almost the same with/without irradiation with visible light, greater antibacterial activity of the tested NRs under irradiation conditions is due to their catalytic production of ROS.

Conclusion

Te-TiO_2 NRs and Se_n/Te-TiO_2 NRs with exposed {100} facets were prepared and tested as efficient photocatalysts and antibacterial agents against *E. coli* and *S. aureus*. By doping Se and Te onto the TiO_2 NRs, the photocatalytic activity towards the production of ·OH increased as a result of an increase in the UV/Vis absorption. In addition to the generation of ROS, the released TeO_3^{2-} and SeO_3^{2-} ions were responsible for enhancing the antibacterial activity of the Se_n/Te-TiO_2 NRs. Relative to commercial TiO_2 NPs, the Te-TiO_2 NRs and $Se_{0.07}$/Te-TiO_2 NRs provide 2.5- and 4.5-fold higher photocatalytic activities. The low cost and high efficiency $Se_{0.07}$/Te-TiO_2 NRs are quite stable and biocompatible, thus showing great practical potential as new and efficient antibacterial agents.

Experimental Section

Preparation of Na-titanate nanotubes

P25 powder (1 g) was added to an aqueous solution of NaOH (10 M, 40 mL), and then transferred to a stainless-steel autoclave (50 mL) lined with Teflon. The sealed autoclave was heated in an oven at 200 °C for 24 hours, and then cooled in air. The obtained solution of Na-titanate nanotubes was subjected to three cycles of centrifugation and washing; centrifugation was conducted at 8000 rpm (Hettich Universal 32R, Tuttlingen, Germany) for 10 minutes and ultrapure water (40×3 mL) was used to wash the pellets.

Synthesis of anatase Te-TiO_2 NRs

The tellurite (TeO_3^{2-}; 10 mM) ions were prepared by dissolving TeO_2 powder (0.064 g) in an aqueous solution of NaOH (20 mM, 40 mL). The as-prepared Na-titanate nanotubes were dispersed into a solution of TeO_3^{2-} (40 mL). After 30 minutes, the mixture was subjected to three cycles of centrifugation (8000 rpm, 10 min) and washed (40×3 mL ultrapure water) to obtain tellurite ions adsorbed on Na-titanate nanotubes. The pellet was dispersed in ultrapure water (40 mL) and then $NaBH_4$ solution (10 mM, 5 mL) was added to the solution of TeO_3^{2-} adsorbed Na-titanate nanotubes during magnetic stirring. After 10 minutes, the mixture was subjected to three cycles of centrifugation (8000 rpm, 10 min) and washed (40×3 mL ultrapure water) to obtain Te-titanate nanotubes. To prepare Te-TiO_2 NRs, the Te-titanate nanotubes were dispersed in deionized water (40 mL) and then transferred to a stainless-steel autoclave (50 mL) lined with Teflon. The sealed autoclave was heated in an oven at 200 °C for 24 hours, and then cooled in air.

Synthesis of anatase Se_n/Te-TiO_2 NRs

The selenite (SeO_3^{2-}) solution (100 mM) was prepared by dissolving SeO_2 powder (0.44 g) in ultrapure water (40 mL). The as-prepared Te-TiO_2 NMs were dispersed in water (40 mL). Aliquots of SeO_3^{2-} solution were added to the as-prepared Te-TiO_2 solutions (each 40 mL), with final SeO_3^{2-} concentrations of 2, 5, and 10 mM. After 30 minutes, the mixtures were subjected to three cycles of centrifugation (8000 rpm, 10 min) and washed (40×3 mL ultrapure water) to obtain selenite ions adsorbed Te-TiO_2 NRs. The pellets were separately dispersed in ultrapure water (40 mL). Then aliquots (10 mM, 5 mL) of $NaBH_4$ solution were separately added into the solutions under magnetic stirring. After 10 minutes, the mixtures were subjected to three cycles of centrifugation (8000 rpm, 10 min) and washed (40×3 mL ultrapure water) to obtain brown Se_n/Te-TiO_2 NRs.

Photocatalytic activity measurement

The photocatalytic activities of the as-prepared Te-TiO_2 NRs, Se_n/Te-TiO_2 NRs, and commercial TiO_2 NPs were evaluated by determining the production of ·OH in aqueous solutions at ambient temperature. The NMs (5 mg) were separately suspended in NaOH solution (10 mM, 10 mL) containing terephthalic acid (3.0 mM). The mixtures were stirred in the dark for 30 minutes, allowing the mixtures to reach equilibrium before irradiation with visible light using a 450-W xenon arc lamp equipped with a 420 nm cutoff filter. The light source was positioned 30 cm above the mixtures. During the photoreactions, no oxygen was bubbled into the suspensions. Aliquots (1.0 mL) of the solutions were taken out every 20 minutes. After being subjected to centrifugation (8000 rpm, 10 min), the fluorescence spectra (excitation wavelength 320 nm) of the supernatants were recorded.

Antibacterial test

E. coli DH5α and *S. aureus* were grown in sterile LB media. The media were prepared by dissolving bacto-tryptone (2.5 g), bacto-yeast extract (1.25 g), and NaCl (2.5 g) in H_2O (250 mL), which was then adjusted to pH 7.0 by adding NaOH (5.0 M). A single colony of each strain was lifted from an LB agar plate and inoculated in LB media (10 mL). The cultures were then grown overnight until the absorbance at the wavelength 600 nm (A_{600}) reached 1.0. A portion of each of the cell mixtures (1 mL) was centrifuged (4000 rpm, 10 min) and washed three times with 0.85% sodium chloride (3×1 mL) to remove the matrix. Cells diluted to 4.0×10^8 CFU mL^{-1} were treated in LB media with/without one of the NMs (Te-TiO_2 NRs, Se_n/Te-TiO_2 NRs, and TiO_2 NPs; 100 μg mL^{-1}), which were either irradiated using visible light (60 min) or not. The viability assay was conducted using SYTO 9 (6 μM) and propidium iodide (PI; 30 μM) stains. Each of the cell samples was then subjected to three cycles of centrifugation/washing to remove the matrix; centrifugation at 4000 rpm for 10 minutes; wash with 0.85% sodium chloride (3×1 mL). Each of the bacterial suspension (100 μL) was

dispensed in a 96-well plate, and then the dye mixture (100 μL) was added to each well. The mixtures were incubated for 15 minutes at ambient temperature. Fluorescence intensities of SYTO 9 (green; excitation wavelength: 475 nm, emission wavelength: 530 nm) and PI (red; excitation wavelength: 475 nm, emission wavelength: 640 nm) were recorded. The green/red fluorescence intensity ratio was used to calculate the ratio of live/dead cells.

Acknowledgements

This study was supported by the National Science Council of Taiwan under contract NSC 101–2113-M-002–002-MY3. Z.-H.L. is grateful to the National Science Council for a postdoctoral fellowship in the Department of Chemistry, National Taiwan University, under contract number NSC 100–2811-M-002–109.

Keywords: antibacterial agents · nanostructures · photocatalysis · selenium · tellurium · titanium dioxide

[1] B. O'Regan, M. Grätzel, *Nature* **1991**, *353*, 737 – 740.
[2] X. Chen, S. S. Mao, *Chem. Rev.* **2007**, *107*, 2891 – 2959.
[3] Z. Yang, C. Y. Chen, P. Roy, H. T. Chang, *Chem. Commun.* **2011**, *47*, 9561 – 9571.
[4] M. R. Hoffmann, S. T. Martin, W. Choi, D. W. Bahnemann, *Chem. Rev.* **1995**, *95*, 69 – 96.
[5] J. Li, L. W. Wang, *Nano Lett.* **2003**, *3*, 1357 – 1363.
[6] W. Guo, C. Xu, X. Wang, S. Wang, C. Pan, C. Lin, Z. L. Wang, *J. Am. Chem. Soc.* **2012**, *134*, 4437 – 4441.
[7] H. G. Yang, C. H. Sun, S. Z. Qiao, J. Zou, G. Liu, S. C. Smith, H. M. Cheng, G. Q. Lu, *Nature* **2008**, *453*, 638 – 641.
[8] A. L. Linsebigler, G. Lu, J. T. Yates, *Chem. Rev.* **1995**, *95*, 735 – 758.
[9] M. Calatayud, C. Minot, *Surf. Sci.* **2004**, *552*, 169 – 179.
[10] M. Lazzeri, A. Vittadini, A. Selloni, *Phys. Rev. B* **2001**, *63*, 155409.
[11] B. Wu, C. Guo, N. Zheng, Z. Xie, G. D. Stuck, *J. Am. Chem. Soc.* **2008**, *130*, 17563 – 17567.
[12] X. Zhao, W. Jin, J. Cai, J. Ye, Z. Li, Y. Ma, J. Xie, L. Qi, *Adv. Funct. Mater.* **2011**, *21*, 3554 – 3563.
[13] J. Li, D. Xu, *Chem. Commun.* **2010**, *46*, 2301 – 2303.
[14] J. Joo, S. G. Kwon, T. Yu, M. Cho, J. Lee, J. Yoon, T. Hyeon, *J. Phys. Chem. B* **2005**, *109*, 15297 – 15302.
[15] X. Wu, Z. Chen, G. Q. Lu, L. Wang, *Adv. Funct. Mater.* **2011**, *21*, 4167 – 4172.
[16] A. El Ruby Mohamed, S. Rohani, *Energy Environ. Sci.* **2011**, *4*, 1065.
[17] P. O. Andersson, C. Lejon, B. Ekstrand-Hammarström, C. Akfur, L. Ahlinder, A. Bucht, L. Österlund, *Small* **2011**, *7*, 514 – 517.
[18] R. Landsiedel, L. Ma-Hock, A. Kroll, D. Hahn, J. Schnekenburger, K. Wiench, W. Wohlleben, *Adv. Mater.* **2010**, *22*, 2601 – 2627.
[19] X. Zong, Z. Xing, H. Yu, Z. Chen, F. Tang, J. Zou, G. Q. Lu, L. Wang, *Chem. Commun.* **2011**, *47*, 11742 – 11744.
[20] J. Yu, G. Dai, Q. Xiang, M. Jaroniec, *J. Mater. Chem.* **2011**, *21*, 1049 – 1057.
[21] L. Zhao, H. Wang, K. Huo, L. Cui, W. Zhang, H. Ni, Y. Zhang, Z. Wu, P. K. Chu, *Biomaterials* **2011**, *32*, 5706 – 5716.
[22] P. V. AshaRani, G. Low Kah Mun, M. P. Hande, S. Valiyaveettil, *ACS Nano* **2009**, *3*, 279 – 290.
[23] P. A. Tran, T. J. Webster, *Int. J. Nanomed.* **2011**, *6*, 1553 – 1558.
[24] Z.-H. Lin, C.-H. Lee, H.-Y. Chang, H.-T. Chang, *Chem. Asian J.* **2012**, *7*, 930 – 934.
[25] T. Kasuga, M. Hiramatsu, A. Hoson, T. Sekino, K. Niihara, *Langmuir* **1998**, *14*, 3160 – 3163.
[26] G. H. Du, Q. Chen, R. C. Che, Z. Y. Yuan, L. M. Peng, *Appl. Phys. Lett.* **2001**, *79*, 3702 – 3704.
[27] D. V. Bavykin, V. N. Parmon, A. A. Lapkin, F. C. Walsh, *J. Mater. Chem.* **2004**, *14*, 3370 – 3377.
[28] E. M. Rockafellow, J. M. Haywood, T. Witte, R. S. Houk, W. S. Jenks, *Langmuir* **2010**, *26*, 19052 – 19059.
[29] Z. H. Lin, C. Chris Wang, *Mater. Chem. Phys.* **2005**, *92*, 591 – 594.
[30] N. R. de Tacconi, C. R. Chenthamarakshan, K. Rajeshwar, E. J. Tacconi, *J. Phys. Chem. B* **2005**, *109*, 11953 – 11960.
[31] A. Pine, G. Dresselhaus, *Phys. Rev. B* **1971**, *4*, 356 – 371.
[32] B. Gates, B. Mayers, B. Cattle, Y. Xia, *Adv. Funct. Mater.* **2002**, *12*, 219 – 227.
[33] J. M. Wu, *J. Mater. Chem.* **2011**, *21*, 14048 – 14055.
[34] A. Samal, T. Pradeep, *J. Phys. Chem. C* **2009**, *113*, 13539 – 13544.
[35] W.-J. Lan, S.-H. Yu, H.-S. Qian, Y. Wan, *Langmuir* **2007**, *23*, 3409.
[36] V. Štengl, S. Bakardjieva, J. Bludská, *J. Mater. Sci.* **2011**, *46*, 3523 – 3536.
[37] J. Pan, G. Liu, G. Q. Lu, H.-M. Cheng, *Angew. Chem.* **2011**, *123*, 2181 – 2185; *Angew. Chem. Int. Ed.* **2011**, *50*, 2133 – 2137.
[38] S. Liu, J. Yu, B. Cheng, *Adv. Colloid Interface Sci.* **2012**, *173*, 35 – 53.
[39] X. Yang, C. Cao, K. Hohn, L. Erickson, R. Maghirang, D. Hamal, K. Klabunde, *J. Catal.* **2007**, *252*, 296 – 302.
[40] G. Liu, H. G. Yang, X. Wang, M. Cheng, J. Pan, G. Q. Lu, H.-M. Cheng, *J. Am. Chem. Soc.* **2009**, *131*, 12868 – 12869.
[41] M. Harb, P. Sautet, P. Raybaud, *J. Phys. Chem. C* **2011**, *115*, 19394 – 19404.
[42] T. Hirakawa, Y. Nosaka, *Langmuir* **2002**, *18*, 3247 – 3254.
[43] G. Mugesh, W. W. Mont, H. Sies, *Chem. Rev.* **2001**, *101*, 2125 – 2179.
[44] A. Simon-Deckers, S. Loo, M. Mayne-L'hermite, N. Herlin-Boime, N. Menguy, C. Reynaud, B. Gouget, M. Carrie're, *Environ. Sci. Technol.* **2009**, *43*, 8423 – 8429.
[45] T. G. Chasteen, R. Bentley, *Chem. Rev.* **2003**, *103*, 1 – 25.

Received: October 30, 2012
Published online on January 21, 2013